Energy dependence of the neutron capture cross section on ^{70}Zn near the inelastic scattering threshold

Rebecca Pachuau,[1] B. Lalremruata,[1,*] N. Otuka,[2] S. V. Suryanarayana,[3] L. R. M. Punte,[1] L. R. Hlondo,[1] V. V. Desai,[3,†] B. Satheesh,[1,‡] S. Kailas,[3] S. Ganesan,[4] B. K. Nayak,[3] and A. Saxena[3]

[1]*Department of Physics, Mizoram University, Tanhril 796004, Aizawl, India*

[2]*Nuclear Data Section, Division of Physical and Chemical Sciences, Department of Nuclear Science and Application, International Atomic Energy Agency, Wien A-1400, Austria*

[3]*Nuclear Physics Division, BARC, Mumbai 40085, India*

[4]*Reactor Physics Design Division, BARC, Mumbai 40085, India*

(Received 18 April 2018; published 28 June 2018; corrected 25 July 2018)

The ^{70}Zn$(n,\gamma)^{71}$Zn^{m} ($T_{1/2} = 3.96$ h) cross section has been measured at 0.40 ± 0.15 MeV and 0.70 ± 0.10 MeV using a ^{7}Li$(p,n)^{7}$Be neutron source. The energy of proton energy of neutron energy spectrum code was used to calculate the neutron energy spectrum, and the ^{197}Au$(n,\gamma)^{198}$Au reaction was used as monitor reaction. Detailed uncertainty analysis has been performed, and the newly measured cross sections are reported with their uncertainties and correlation coefficients. The energy dependence seen in the cross sections measured in the present work and in the previous work at higher energies has been compared with the theoretical model prediction with various level density models and γ-ray strength functions. Model code dependence of the prediction is also discussed.

DOI: 10.1103/PhysRevC.97.064617

I. INTRODUCTION

The neutron-induced reactions on zinc isotopes have many practical interests in nuclear science and engineering. ^{70}Zn is one of the signatures of the *s*-process during shell carbon burning in massive stars, and its overabundance can also be used as an indicator of the strength of the nuclear reaction flow through the branching along the *s*-process path, especially the branching at ^{69}Zn [1].

In spite of its importance, there has not been a measured ^{70}Zn$(n,\gamma)^{71}$Zn cross section in the fast neutron energy region in the EXFOR library [2] except for the ^{70}Zn$(n,\gamma)^{71}$Zn^{m} ($T_{1/2} = 3.96$ h) cross sections at 0.96 MeV and 1.69 MeV [3,4] though there are a number of measurements for thermal neutrons [5–9] as well as $kT \sim 25$ keV neutrons [10]. The ^{70}Zn$(n,\gamma)^{71}$Zn cross section should decrease very rapidly when the incident neutron energy crosses the ^{70}Zn$(n,n_1)^{70}$Zn inelastic scattering threshold energy (885 keV). The rapid decrease is predicted by TALYS [11]. The present work focuses on the energy dependence of the ^{70}Zn$(n,\gamma)^{71}$Zn^{m} cross section around this inelastic scattering threshold by measuring the cross sections at 0.40 and 0.70 MeV, and tests theoretical predictions by TALYS against the measured cross sections.

II. DETAILS OF EXPERIMENT

A. Neutron source

The experiment was carried out at the Folded Tandem Ion Accelerator (FOTIA) Facility, Bhabha Atomic Research Centre (BARC), Mumbai. The neutron beam was obtained from the ^{7}Li$(p,n)^{7}$Be reaction. The energies of proton beam were 2.25 MeV and 2.60 MeV with energy spread of ± 0.02 MeV. The thickness of the lithium targets used for irradiation at 2.25 and 2.60 MeV proton energies were 2.0 mg/cm^2 (37.4 μm) and 2.5 mg/cm^2 (46.8 μm) respectively. The proton beam current during irradiation varied from 50–100 nA, and the beam diameter on the lithium target was about 5 mm. A 0.25-mm-thick tantalum foil (manufactured by Goodfellow Cambridge Limited, United Kingdom and supplied by H. Fillunger & Co. Pvt. Ltd., Bangalore) on which the lithium target was pasted was used as a proton beam stopper. The time structure of the neutron flux was monitored online by a NE213 neutron detector at 0° and at 1-m distance from the lithium target. The neutron flux was recorded and saved every 30 min to get the neutron flux fluctuation during the whole irradiation period.

Subtractions of the (p,n_1) and breakup neutron contributions are always an essential part in experimental determination of neutron-induced reaction cross section with a ^{7}Li(p,n) neutron source when the proton beam energy is above the (p,n_1) threshold at 2.37 MeV. The time-of-flight and multiple foil activation techniques cannot be applied at BARC-FOTIA due to the continuous beam structure and weak neutron flux. Therefore, energy of proton energy of neutron (EPEN) [12] neutron energy spectrum code developed by our group was used to calculate the ^{7}Li$(p,n)^{7}$Be neutron energy spectra.

*Corresponding author: marema08@gmail.com

†Present address: Nuclear Chemistry, Oregon State University, Corvallis, Oregon 97331, USA.

‡Present address: Department of Physics, Mahatma Gandhi. Govt. Arts College, Chalakkara, New Mahe 673311, U.T. of Puducherry, India.

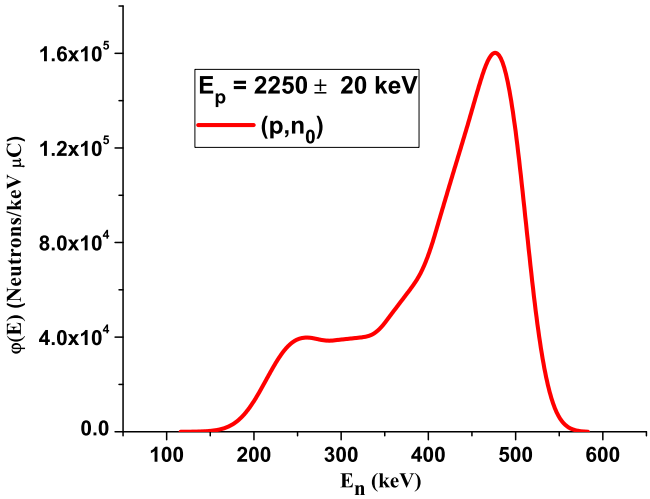

FIG. 1. Neutron flux energy spectrum $\varphi(E)$ from the ^{7}Li$(p,n_0)^{7}$Be reaction at $E_p = 2.25 \pm 0.02$ MeV obtained from the code EPEN [12].

Figures 1 and 2 show the neutron flux energy spectra for a 1 cm×1 cm square activation sample placed at 1.4 cm from a lithium target calculated by EPEN at proton energies 2.25 ± 0.02 MeV and 2.60 ± 0.02 MeV, respectively. Their numerical data can be obtained at the EPEN web interface [13]. The spectrum averaged (p,n_0) neutron energies obtained from these EPEN spectra were 0.40 ± 0.15 MeV and 0.70 ± 0.10 MeV for $E_p = 2.25$ and 2.60 MeV, respectively.

B. Sample preparation

A metallic zinc foil enriched ($72.4 \pm 1.0\%$) to ^{70}Zn was sandwiched between gold foils. The gold foils were used for normalization of the measured cross section with the ^{197}Au$(n,\gamma)^{198}$Au standard cross section. A natural indium foil was also stacked at the end of the foil stack to serve as an independent flux monitor foil using the ^{115}In$(n,n')^{115}$In^{m}

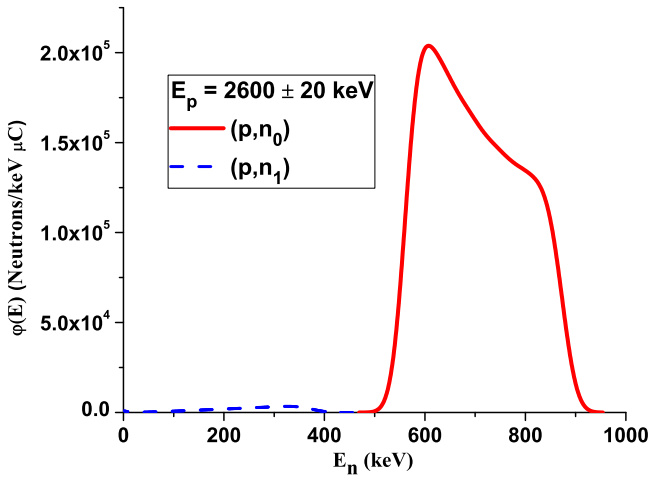

FIG. 2. Neutron flux energy spectrum $\varphi(E)$ from the ^{7}Li$(p,n_0)^{7}$Be and ^{7}Li$(p,n_1)^{7}$Be reaction at $E_p = 2.60 \pm 0.02$ keV obtained from the code EPEN [12].

TABLE I. Details of foils used in the present experiment.

Isotope	Enrichment (%)	Purity (%)	E_n (MeV)	Thickness (mg/cm^2)
^{70}Zn	72.4 ± 1.0 8.49 (^{64}Zn) 8.40(^{66}Zn) 2.01(^{67}Zn) 8.70(^{68}Zn)	>99.97	0.40 0.70	113.6 ± 0.1
^{197}Au	100%	99.95	0.40	54.2 ± 0.1 (front) 52.6 ± 0.1 (back)
			0.70	72.3 ± 0.1 (front) 68.5 ± 0.1 (back)
^{115}In	95.71%	99.99	0.40 0.70	129.8 ± 0.1

reaction for cross checking. The sample stack (1 cm × 1 cm) was placed at 1.4 cm distance from the lithium target. Details about the foils used in the experiment are summarized in Table I.

C. Measurement of γ-ray activity

The γ-ray activity of the foils was measured using a precalibrated lead-shielded 185-cc high-purity germanium (HPGe) detector having 30% relative efficiency and 1.8-keV energy resolution at 1.33-MeV γ energy. For each incident energy, the activities of the stacks of the foils were counted together, not the individual foils separately. The data acquisition was carried out using CAMAC-based Linux Advanced Multiparameter System software (TCAMCON-95/CC 2000 crates controller and CM-48 ADCs), where the detector dead time was negligible. To correctly identify the γ ray of interest, the decay curve analysis was carried out by saving the γ count periodically and followed for two to three times the half-life of ^{71}Zn^{m} as shown in Table II.

Detailed explanation and discussion of the HPGe detector efficiency calibration including uncertainty propagation to the parameters characterizing the efficiency curve are explained in our previous report [3,4,17,18], and the same parameters and their correlation coefficients are adopted in the present work.

III. DATA ANALYSIS PROCEDURE

The spectrum averaged cross section for ^{70}Zn$(n,\gamma)^{71}$Zn^{m} was calculated using the standard activation formula

$$\langle \sigma_{\mathrm{Zn}}^{\mathrm{m}} \rangle = \langle \sigma_{\mathrm{Au}} \rangle (A_{\mathrm{Zn}}/A_{\mathrm{Au}})[(a_{\mathrm{Au}} n_{\mathrm{Au}} I_{\mathrm{Au}} \varepsilon_{\mathrm{Au}} f_{\mathrm{Au}})/ (a_{\mathrm{Zn}} n_{\mathrm{Zn}} I_{\mathrm{Zn}} \varepsilon_{\mathrm{Zn}} f_{\mathrm{Zn}})](C_{\mathrm{Zn}}/C_{\mathrm{Au}}), \quad (1)$$

where, $A_x = \Sigma_i A_{x,i}$ is the number of counts ($A_{x,i}$ is the number of counts from ith counting), a_x is the isotopic abundance of the sample, n_x is the number of atoms, I_x is the γ intensity, ε_x is the detection efficiency,

$$f_x = [1 - \exp(-\lambda_x t_1)] \sum_i \exp(-\lambda_x t_{2,i}) \times [1 - \exp(-\lambda_x t_{3,i})]/\lambda_x \quad (2)$$

TABLE II. Irradiation, cooling, and counting times.

E_n (MeV)	Irradiation time (sec.)	Counting No.	Cooling time (sec.) (beam stop time-counting start time)	Counting time (sec.)
0.40	14760.0	1	2428.0	3776.7
		2	6210.7	7232.1
		3	13450.8	7216.7
		4	20674.5	7306.3
		5	27989.8	7235.1
		6	35233.9	2551.8
0.70	18924.0	1	1127.0	1983.7
		2	3115.7	1804.9
		3	6623.0	1804.4
		4	8434.4	1760.6
		5	10381.0	3599.9
		6	13987.9	3600.0

is the timing factor (for the irradiation time t_1, cooling time for the ith counting $t_{2,\mathrm{i}}$, measuring time for the ith counting $t_{3,\mathrm{i}}$), λ_x is the decay constant, and C_x is the correction factor ($x =$ Zn or Au). The timing parameters and decay data are given in Tables II and III, respectively.

The ^{197}Au$(n,\gamma)^{198}$Au reaction was used as the neutron flux monitor. Since the incident neutron beam of ^{7}Li$(p,n_0)^{7}$Be is not monoenergetic, the energy-dependent monitor cross section in the IAEA Neutron Cross-Section Standards was folded by the neutron energy spectrum obtained from EPEN by

$$\langle\sigma_{\mathrm{Au}}\rangle = \int \varphi(E)\sigma_{\mathrm{Au}}(E)dE, \tag{3}$$

where φ is the neutron flux energy spectrum obtained from EPEN (normalized to $\int \varphi(E)dE = 1$) and $\sigma_{\mathrm{Au}}(E)$ is the pointwise ^{197}Au$(n,\gamma)^{198}$Au cross section obtained from the IAEA Neutron Cross-Section Standards [19]. The energy integral is taken over the energy range where (p,n_0) neutrons exist.

In the present work, the correction factor C_x in Eq. (1) is decomposed to $C_x = C_{x,\mathrm{fluc}}C_{x,\mathrm{low}}C_{x,\mathrm{scat}}C_{x,\mathrm{attn.}}$.

Each term is the correction factor for

(i) neutron flux fluctuation (fluc),
(ii) low-energy neutron background due to ^{7}Li$(p,n_1)^{7}$Be neutrons (low),
(iii) scattered neutron background originating from elastic, inelastic, and multiple scatterings in the foil stack and surrounding materials (scat),
(iv) γ-ray self-attenuation (attn),

whose detailed descriptions are given in our previous report [3,4]. C_{scat} was calculated by the Monte Carlo transport code PHITS, Ver. 3.000 [20]. The values of the correction factors are summarized in Table IV. Note that $C_{x,\mathrm{low}} = 1$ at 0.40 MeV due to absence of the (p,n_1) neutrons at this energy.

TABLE III. Decay data adopted in the present work taken from the ENSDF library [14–16].

Nuclide	Half-life	E_γ (keV)	I_γ (%)
^{71}Zn$^{\mathrm{m}}$	3.96 ± 0.05 h	386.280	91.40 ± 2.10
^{198}Au	2.6947 ± 0.0003 d	411.802	95.62 ± 0.06
^{115}In$^{\mathrm{m}}$	4.486 ± 0.004 h	336.240	45.80 ± 2.20

IV. UNCERTAINTY PROPAGATION

Following our earlier work [3,4,17], the fractional uncertainty and correlation in the measured cross section was propagated from the fractional uncertainties in $\langle\sigma_{\mathrm{Au}}\rangle$, A_x, a_x, n_x, I_x, f_x, and $\eta = \varepsilon_{\mathrm{Au}}/\varepsilon_{\mathrm{Zn}}$. The fractional uncertainty in f_x was propagated from the uncertainty in $T_{1/2}$ assuming that the uncertainties in irradiation, cooling, and measuring times are negligible.

We also estimated correlation coefficients among the cross sections measured in this work (0.40 and 0.70 MeV) and in the previous report (0.96 and 1.69 MeV [3,4]). It is obvious that A_x is uncorrelated while a_x, I_x, f_x, and η are fully correlated. n_{Zn} is fully correlated between 0.40, 0.70, and 1.69 MeV but they are uncorrelated with the measurement at 0.96 MeV because we used the 87.3 mg/cm^2–thick Zn foil at 0.96 MeV while the 113.6 mg/cm^2 Zn foil at the other energies. n_{Au} is uncorrelated because we used different Au foils at different energies.

The fractional uncertainty and correlation in $\langle\sigma_{\mathrm{Au}}\rangle$ were obtained as described in our previous report [17,18], where the covariances of the 11 groupwise cross sections (covering

TABLE IV. Correction factors applied to the measured cross sections.

E_n (MeV)	0.40	0.70
$C_{\mathrm{Zn,fluc}}/C_{\mathrm{Au,fluc}}$	0.888	0.939
$C_{\mathrm{Au,low}}$	1	0.967
$C_{\mathrm{Zn,low}}$	1	0.988
$C_{\mathrm{Zn,scat}}$	0.980	0.984
$C_{\mathrm{Au,scat}}$	0.981 (front)	0.983 (front)
	0.978 (back)	0.980 (back)
	0.980 (mean)	0.982 (mean)
$C_{\mathrm{Zn,attn}}$	1.019	1.021
$C_{\mathrm{Au,attn}}$	1.024 (front)	1.028 (front)
	1.013 (back)	1.015 (back)
	1.019 (mean)	1.022 (mean)

TABLE V. Groupwise fractional neutron fluxes, monitor cross sections, and their corresponding uncertainties for $\langle E_n \rangle = 0.40$, 0.70, 0.96, and 1.69 MeV adopted in the present work.

Group k	$E_{\min}$ (MeV)	$E_{\max}$ (MeV)	σ_k (mb)	$\Delta\sigma_k$ (%)	$\Phi_{i,k}/\sum\Phi_{i,k}$			
					0.40 MeV ($i=1$)	0.70 MeV ($i=2$)	0.96 MeV ($i=3$)	1.69 MeV ($i=4$)
18	0.0900	0.0975	324.56	0.98	7.139×10^{-08}			
19	0.0975	0.1100	314.64	1.02	6.948×10^{-06}			
20	0.1100	0.1350	293.85	0.96	2.300×10^{-04}			
21	0.1350	0.1600	277.02	0.99	1.913×10^{-03}			
22	0.1600	0.1750	266.89	1.14	4.067×10^{-03}			
23	0.1750	0.1850	262.62	2.30	5.133×10^{-03}			
24	0.1850	0.1950	256.99	1.35	7.717×10^{-03}			
25	0.1950	0.2050	252.97	1.40	1.053×10^{-02}			
26	0.2050	0.2150	249.01	1.29	1.313×10^{-02}			
27	0.2150	0.2250	246.78	1.31	1.515×10^{-02}			
28	0.2250	0.2325	243.96	1.58	1.308×10^{-02}			
29	0.2325	0.2375	239.11	1.29	8.423×10^{-03}			
30	0.2375	0.2425	236.41	1.83	8.509×10^{-03}			
31	0.2425	0.2475	236.86	1.27	8.523×10^{-03}			
32	0.2475	0.2550	236.70	1.38	1.185×10^{-02}			
33	0.2550	0.2650	235.67	1.31	1.658×10^{-02}			
34	0.2650	0.2750	230.12	1.63	1.604×10^{-02}			
35	0.2750	0.2900	215.25	1.29	2.334×10^{-02}			
36	0.2900	0.3125	198.89	1.17	3.603×10^{-02}			
37	0.3125	0.3375	188.45	1.15	4.033×10^{-02}			
38	0.3375	0.3625	178.70	1.07	4.684×10^{-02}			
39	0.3625	0.3875	169.55	1.05	5.890×10^{-02}			
40	0.3875	0.4125	162.43	1.03	7.684×10^{-02}			
41	0.4125	0.4375	154.97	1.18	1.066×10^{-01}			
42	0.4375	0.4625	146.65	1.00	1.376×10^{-01}			
43	0.4625	0.4875	141.56	1.06	1.579×10^{-01}	1.037×10^{-05}		
44	0.4875	0.5100	136.90	1.05	1.115×10^{-01}	3.881×10^{-04}		
45	0.5100	0.5300	130.30	1.10	4.825×10^{-02}	3.383×10^{-03}		
46	0.5300	0.5550	124.49	1.18	1.393×10^{-02}	2.350×10^{-02}		
47	0.5550	0.5850	119.09	1.51	1.037×10^{-03}	8.302×10^{-02}		
48	0.5850	0.6250	108.87	1.08		1.563×10^{-01}		
49	0.6250	0.6750	100.47	1.26		1.816×10^{-01}		
50	0.6750	0.7250	96.23	1.13		1.590×10^{-01}	5.730×10^{-10}	
51	0.7250	0.7750	93.81	1.30		1.424×10^{-01}	2.746×10^{-05}	
52	0.7750	0.8250	88.93	1.05		1.311×10^{-01}	9.641×10^{-03}	
53	0.8250	0.8750	85.57	1.63		9.894×10^{-02}	1.231×10^{-01}	
54	0.8750	0.9200	84.70	2.18		1.992×10^{-02}	1.975×10^{-01}	
55	0.9200	0.9500	85.22	1.93		4.215×10^{-04}	1.314×10^{-01}	
56	0.9500	0.9700	85.23	4.24		8.025×10^{-07}	8.559×10^{-02}	
57	0.9700	0.9900	84.97	3.18			8.430×10^{-02}	
58	0.9900	1.0500	79.71	1.04			2.438×10^{-01}	
59	1.0500	1.1750	77.63	1.39			1.247×10^{-01}	
60	1.1750	1.3250	73.84	1.26			2.884×10^{-07}	
61	1.3250	1.5000	70.88	1.72				1.018×10^{-06}
62	1.5000	1.7000	67.41	1.51				5.295×10^{-01}
63	1.7000	1.9000	60.17	2.04				4.705×10^{-01}
64	1.9000	2.1000	52.62	1.63				3.030×10^{-08}

0.96 ± 0.15 MeV neutrons) and four groupwise cross sections (covering 1.69 ± 0.15 MeV neutrons) in the IAEA Neutron Cross-Section Standards [19] were used to propagate the covariance of the spectrum averaged ^{197}Au$(n,\gamma)^{198}$Au cross sections at these two neutron energies. In the present work, this procedure is extended to the other two neutron energies by using the covariance of the 30 groupwise cross sections (covering 0.40 ± 0.15 MeV neutrons) and 14 groupwise cross sections (covering 0.70 ± 0.10 MeV neutrons) in the IAEA Neutron Cross-Section Standards. If we denote fraction of the neutrons in the kth group by $\Phi_{i,k} = \int_k \varphi_i(E)dE$ ($i = 1$ for 0.40 MeV, $i = 2$ for 0.70 MeV, etc., $\int_k$ means integral over

TABLE VI. Spectrum-averaged monitor cross sections with their uncertainties and correlation coefficients.

E_n (MeV)	$\langle\sigma_{Au}\rangle$ (mb)	Cor($\langle\sigma_{Au}\rangle_i$, $\langle\sigma_{Au}\rangle_j$)			
0.40	167.16 ± 1.11	1.000			
0.70	99.00 ± 0.77	0.472	1.000		
0.96	82.77 ± 0.86	0.341	0.402	1.000	
1.69	64.09 ± 0.92	0.248	0.217	0.222	1.000

the kth energy group, i.e., $\Sigma_k \Phi_{i,k} = 1$), the spectrum-averaged ^{197}Au$(n,\gamma)^{198}$Au cross section at the ith neutron energy is $\langle\sigma_{Au}\rangle_i = \Sigma_k \Phi_{i,k}\sigma_k$, where σ_k is the kth groupwise cross section in the IAEA Neutron Cross-Section Standards. The absolute variance and covariance of $\langle\sigma_{Au}\rangle_i$ are

$$\mathrm{Var}(\langle\sigma_{Au}\rangle_i) = \Sigma_k \Phi_{i,k}^2 \mathrm{Var}(\sigma_k) + 2\Sigma_{k<l}\Phi_{i,k}\mathrm{Cov}(\sigma_k,\sigma_l)\Phi_{i,l},$$

$$\mathrm{Cov}(\langle\sigma_{Au}\rangle_i,\langle\sigma_{Au}\rangle_j) = \Sigma_{k,l}\Phi_{i,k}\mathrm{Cov}(\sigma_k,\sigma_l)\Phi_{j,l}.$$

The values of $\langle\sigma_k\rangle$ and $\Phi_{i,k}$ are summarized in Table V. These values for two higher neutron energies ($i = 3$ for 0.96 MeV and $i = 4$ for 1.69 MeV) are also provided in Table III of [17] with their correlation coefficients

$$\mathrm{Cor}(\sigma_k,\sigma_l) = \mathrm{Cov}(\sigma_k,\sigma_l)/[\mathrm{Var}(\sigma_k)\mathrm{Var}(\sigma_l)]^{1/2}.$$

Table VI shows the spectrum averaged monitor cross section $\langle\sigma_{Au}\rangle_i$ along with its uncertainty $\Delta\langle\sigma_{Au}\rangle_i = \mathrm{Var}(\langle\sigma_{Au}\rangle_i)^{1/2}$ and correlation coefficients

$$\mathrm{Cor}(\langle\sigma_{Au}\rangle_i, \langle\sigma_{Au}\rangle_j) = \mathrm{Cov}(\langle\sigma_{Au}\rangle_i, \langle\sigma_{Au}\rangle_j)/(\Delta\langle\sigma_{Au}\rangle_i \Delta\langle\sigma_{Au}\rangle_j).$$

Note that the correlation coefficient between 0.96 and 1.69 MeV reported in our previous work (Footnote *b* of Table IX of Ref. [3] and Table IV of Ref. [17]) was 7%. After reanalysis, the correlation coefficient was found to be 22.2% instead of 7% [18] as shown in Table VI**.** The mistake made in our earlier analysis was identified and corrected in the present work. However, this change in the correlation coefficient from 7% to 22.2% does not change the correlation coefficient of 12% between measured neutron capture cross sections for 0.96 and 1.69 MeV reported in our earlier work (Table VIII of Ref. [3]).

Table VII summarizes the overall and partial uncertainties and correlation coefficients in various parameters to obtain the ^{70}Zn$(n,\gamma)^{71}$Zn^m cross section at neutron energies, 0.40, 0.70, 0.96, and 1.69 MeV. From this table, we can construct the fractional uncertainties and correlation coefficients of the ^{70}Zn$(n,\gamma)^{71}$Zn^m cross sections at four neutron energies as described in Sec. 4.1.4 of Ref. [17].

V. NUCLEAR REACTION MODELS

The excitation function of ^{70}Zn$(n,\gamma)^{71}$Zn^m reaction from 0.1–2.5 MeV has been calculated using the nuclear reaction model code TALYS-1.8 [11]. The nuclear models implemented in this code can generally be categorized into optical, direct, preequilibrium, and compound models, which can be used with various buildup parameter options including those compiled in the RIPL-3 Reference Input Parameter Library [21].

The default optical model potentials (OMPs) used in TALYS are based on the local and global parametrizations by Koning and Delaroche [22]. The compound nucleus contribution was calculated by the Hauser-Feshbach model [23]. The following six level density models available in TALYS-1.8 were used:

(i) Level density model 1(LDM-1): the constant temperature and Fermi-gas model where the constant temperature model is used in the low excitation region and the Fermi-gas model is used in the high excitation energy region. The transition energy is around the neutron separation energy.
(ii) Level density model 2(LDM-2): the backshifted Fermi-gas model.
(iii) Level density model 3(LDM-3): the generalized superfluid model.
(iv) Level density model 4(LDM-4): the microscopic level densities (Skyrme force) from Goriely's tables [20].
(v) Level density model 5(LDM-5): the microscopic level densities (Skyrme force) from Hilaire's combinatorial tables [20].
(vi) Level density model 6(LDM-6): the microscopic level densities (temperature-dependent Hartree-Fock-Bolyubov, Gogny force) from Hilaire's combinatorial tables [24].

TABLE VII. Fractional uncertainties (%) and correlation coefficients in various parameters associated with the measured ^{70}Zn$(n,\gamma)^{71}$Zn^m cross sections. Cor(x,y) means the correlation coefficient of the specific uncertainty source between x MeV and y MeV.

E_n (MeV)	A_{Zn}	A_{Au}	a_{Zn}	n_{Zn}	n_{Au}	I_{Zn}	I_{Au}	f_{Zn}	f_{Au}	η	$\langle\sigma_{Au}\rangle$	Total
0.40	5.239	1.996	1.381	0.088	0.131	2.298	0.063	0.244	0.018	0.257	0.679	6.262
0.70	1.410	0.598	1.381	0.088	0.099	2.298	0.063	0.163	0.017	0.257	0.780	3.203
0.96	7.809	3.247	1.381	0.115	0.099	2.298	0.063	0.177	0.027	0.257	1.030	8.940
1.69	5.988	2.471	1.381	0.088	0.097	2.298	0.063	0.273	0.015	0.257	1.461	7.167
Cor(0.40,0.70)	0	0	1	1	0	1	1	1	1	1	0.472	0.373
Cor(0.40,0.96)	0	0	1	0	0	1	1	1	1	1	0.341	0.135
Cor(0.40,1.69)	0	0	1	1	0	1	1	1	1	1	0.248	0.169
Cor(0.70,0.96)	0	0	1	0	0	1	1	1	1	1	0.402	0.262
Cor(0.70,1.69)	0	0	1	1	0	1	1	1	1	1	0.217	0.316
Cor(0.96,1.69)	0	0	1	0	0	1	1	1	1	1	0.222	0.119

TABLE VIII. The ^{70}Zn$(n,\gamma)^{71}$Zn^{m} cross sections measured in the present and previous experiments with their total uncertainties and correlation coefficients.

E_n (MeV)	$\langle\sigma^m_{Zn}\rangle$ (mb)	Correlation coefficients				Ref.
0.40	1.82 ± 0.11	1.00				Present
0.70	1.99 ± 0.06	0.38	1.00			Present
0.96	1.83 ± 0.16	0.13	0.27	1.00		[3,4]
1.69	1.33 ± 0.10	0.17	0.33	0.12	1.00	[3,4]

There are eight different options for the γ-ray strength function in TALYS-1.8 and their sensitivity has been studied. In general, most of these options are based on the work of Kopecky and Uhl [25], or Brink [26] and Axel [27]. The eight different γ-ray strength functions are listed below:

(i) Photon strength function 1(PSF-1): Kopecky-Uhl generalized Lorentzian [25].
(ii) Photon strength function 2(PSF-2): Brink [26] and Axel Lorentzian [27].
(iii) Photon strength function 3(PSF-3): Hartree-Fock BCS tables [21].
(iv) Photon strength function 4(PSF-4): Hartree-Fock-Bogolyubov tables [21].
(v) Photon strength function 5(PSF-5): Goriely's hybrid model [28].
(vi) Photon strength function 6(PSF-6): Goriely temperature-dependent Hartree-Fock-Bogolyubov.
(vii) Photon strength function 7(PSF-7): Temperature-dependent relativistic mean field.
(viii) Photon strength function 8(PSF-8): Gogny D1M Hartree-Fock-Bogolyubov+QRPA.

The theoretical calculations have been performed using the default parameter values except for these level density models and γ-ray strength functions.

VI. RESULTS AND DISCUSSIONS

The ^{70}Zn$(n,\gamma)^{71}$Zn^{m} reaction cross sections newly determined in the present work at neutron energies 0.40 MeV and 0.70 are given in Table VIII along with our earlier measured cross sections at 0.96 MeV and 1.69 MeV [3,4].

The comparison between the measured spectrum-averaged ^{70}Zn$(n,\gamma)^{71}$Zn^{m} reaction cross sections and the cross sections for monoenergetic neutrons calculated by nuclear reaction model code TALYS-1.8 are shown in Fig. 3. This figure shows that the TALYS-1.8 results for all level density models (LDM-1 to LDM-6) with two γ-ray strength functions (PSF-3 and PSF-4) are close to all the experimental cross sections. However, TALYS-1.8 with the generalized superfluid level

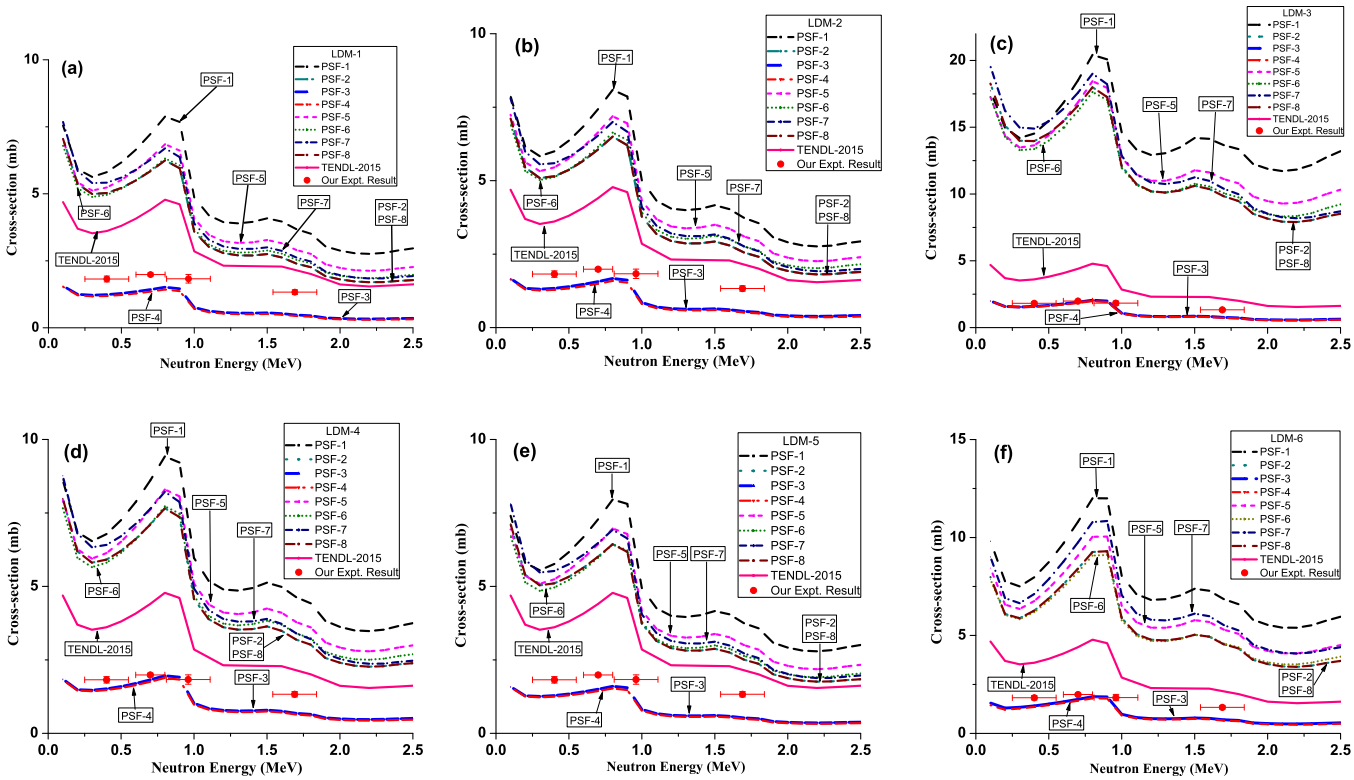

FIG. 3. Excitation functions of the ^{70}Zn$(n,\gamma)^{71}$Zn^{m} cross sections measured by us, evaluated in TENDL-2015 (solid line) as well as predicted by TALYS-1.8 with eight different γ-ray strength functions (PSF-1–8) and the level density models (LDM-1–6): (a) LDM-1, (b) LDM-2, (c) LDM-3, (d) LDM-4, (e) LDM-5, and (f) LDM-6. See the text for the details of these γ-ray strength functions and level density models. The experimental cross sections are (p,n_0) neutron flux energy spectrum averaged, whereas the evaluated and calculated cross sections are for monoenergetic neutrons.

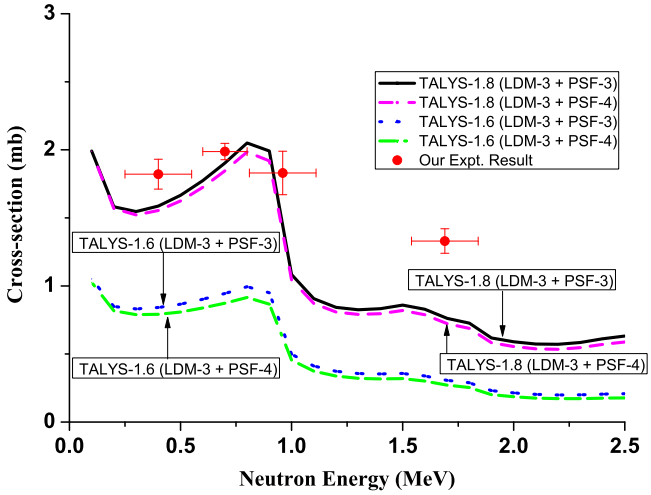

FIG. 4. Comparison between predictions of ^{70}Zn$(n,\gamma)^{71}$Zn^{m} reaction cross sections by TALYS-1.6 and TALYS-1.8 with two different γ-ray strength functions (PSF-3 and PSF-4) and the level density model (LDM-3) respectively.

density model (LDM-3) in Fig. 3(c) best matches the measured cross sections except for 1.69 MeV where the measured cross section is slightly overestimated by TALYS-1.8. It is also worth mentioning that a rapid rise and fall of the capture cross section near the inelastic threshold is predicted by the TALYS-1.8 calculation with all the available level density models and γ-ray strength functions (PSF-1, 2, 5–8) while the TALYS-1.8 calculation with level density models (LDM-1 to LDM-6) and γ-ray strength functions (PSF-3 and PSF-4) predicted a much slower increase and decrease in the capture cross sections around the inelastic threshold, which agrees with the experimental results. It can also be observed from these figures that the prediction of TALYS-1.8 is very sensitive to the choice of the level density models and the γ-ray strength functions.

In order to check the code dependence, the ^{70}Zn$(n,\gamma)^{71}$Zn^{m} reaction cross sections predicted by TALYS-1.8 are also compared with those predicted by TALYS-1.6. The level density model and γ-ray strength functions used in TALYS-1.8 (LDM-3, PSF-3, or PSF-4) are also used in TALYS-1.6. Figure 4 shows that the predictions by TALYS-1.6 are much lower compared to the predictions by TALYS-1.8 even though the same options are chosen. Our previous work [3,4] demonstrates that LDM-3 and PSF-1 (Kopecky-Uhl) are the best combination to reproduce our cross sections at 0.96 and 1.69 MeV by TALYS-1.6.

As the measured cross sections have been determined with their covariances, it is possible to quantify the model prediction capability by estimating

$$\chi^2 = (\sigma_{\rm exp} - \sigma_{\rm mod})^t V^{-1} (\sigma_{\rm exp} - \sigma_{\rm mod}),$$

where $\sigma_{\rm exp}$ and $\sigma_{\rm mod}$ are 1×4 column vectors, which consist of the cross sections at four energies from the experiment and model, respectively, and V is the 4×4 covariance matrix of the measured cross sections. TALYS-1.6 (LDM-3+PSF-1) and TALYS-1.8 (LDM-3+PSF-3) give $\sqrt{(\chi^2/4)} = 6.3$ and 3.4, respectively.

VII. SUMMARY

The ^{70}Zn$(n,\gamma)^{71}$Zn^{m} reaction cross sections have been measured just below and above the inelastic scattering threshold energy using standard activation technique. The ^{7}Li$(p,n)^{7}$Be reaction was used as the neutron source. The neutron energy spectrum code EPEN was used to obtain the neutron flux energy spectra. The data analysis was carried out using the latest decay data in the ENSDF library and ^{197}Au$(n,\gamma)^{198}$Au cross sections in the IAEA Neutron Cross Section Standards. We took into account corrections due to the neutron flux fluctuation, low energy (p,n_1) neutron background, scattered neutron background, and γ self-attenuation. The uncertainty propagation from various sources of the uncertainty and correlation was performed, and the total and partial uncertainties of the measured cross sections were reported with their correlations. The cross section was also calculated by the computer code TALYS-1.8 below and above the inelastic scattering threshold energy. The energy dependence of the calculated cross sections was compared with the energy dependence of the measured cross sections below and above the (n,n_1) threshold. The comparison showed that TALYS-1.8 with the generalized superfluid level model (LDM-3) and Hartree-Fock BCS (PSF-3) or Hartree-Fock-Bogolyubov (PSF-4) γ-ray strength functions best matches the measured cross sections. However, these options are not best combination if we use TALYS-1.6 instead of TALYS-1.8.

ACKNOWLEDGMENTS

The authors would like to thank Dr. Yosuke Iwamoto (Japan Atomic Energy Agency) for his advice on calculation of correction factors for multiple scattering by PHITS. This research was carried out under the joint collaboration research project between the Department of Physics, Mizoram University and BARC, Mumbai under the financial support provided by the B.R.N.S., DAE, Mumbai (Sanction No. 2012/36/17-BRNS Dated 14.08.2012). The authors are grateful to the TIFR, Mumbai for providing the lithium target. The authors also gratefully acknowledge the excellent cooperation of the FOTIA accelerator operators for the smooth operation of the machine throughout the whole experiment. One of the authors (R.P.) is thankful to the University Grant Commission for providing financial support under National Fellowship for Higher Education (Sanction No.: F1-17.1/2015-16/NFST-2015-17-ST-MIZ-2682) to carry out her research work.

[1] L.-S. The, M. F. El Eid, and B. S. Meyer, Astrophys. J. **655**, 1058 (2007).

[2] N. Otuka, E. Dupont, V. Semkova, B. Pritychenko, A. I. Blokhin, M. Aikawa, S. Babykina, M. Bossant, G. Chen, S. Dunaeva, R. A. Forrest, T. Fukahori, N. Furutachi, S. Ganesan, Z. Ge, O. O. Gritzay, M. Herman, S. Hlavač, K. Katō, B. Lalremruata, Y. O. Lee, A. Makinaga, K. Matsumoto, M. Mikhaylyukova, G. Pikulina, V. G. Pronyaev, A. Saxena, O. Schwerer, S. P. Simakov,

N. Soppera, R. Suzuki, S. Takács, X. Tao, S. Taova, F. Tárkányi, V. V. Varlamov, J. Wang, S. C. Yang, V. Zerkin, and Y. Zhuang, Nucl. Data Sheets **120**, 272 (2014).
[3] L. R. M. Punte, B. Lalremruata, N. Otuka, S. V. Suryanarayana, Y. Iwamoto, Rebecca Pachuau, B. Satheesh, H. H. Thanga, L. S. Danu, V. V. Desai, L. R. Hlondo, S. Kailas, S. Ganesan, B. K. Nayak, and A. Saxena, Phys. Rev. C **95**, 024619 (2017).
[4] B. Lalremruata, L. R. M. Punte, N. Otuka, R. Pachuau, Y. Iwamoto, S. V. Suryanarayana, B. K. Nayak, B. Satheesh, H. H. Thanga, L. S. Danu, V. V. Desai, L. R. Hlondo, S. Kailas, S. Ganesan, and A. Saxena, International Atomic Energy Agency Report No. INDC(IND)-0049, 2017.
[5] D. Hughes (private communication).
[6] S. K. Mangal and P. S. Gill, Nucl. Phys. **36**, 542 (1962).
[7] H. Arino, H. H. Kramer, V. J. Molinski, R. S. Tilsbury, W. H. Wahl, and P. M. Stier, US Atomic Energy Commission Report NYO-10175, 1964.
[8] W. Mannhart and H. K. Vonach, Z. Phys. **210**, 13 (1968).
[9] K. S. Krane, Appl. Radiat. Isotopes **121**, 28 (2017).
[10] R. Reifarth, S. Dababneh, M. Heil, F. Käppeler, R. Plag, K. Sonnabend, and E. Uberseder, Phys. Rev. C **85**, 035802 (2012).
[11] A. J. Koning, S. Hilaire, and M. C. Duijvestijn, in *Proceedings of the International Conference on Nuclear Data for Science and Technology, 2007, Nice, France*, edited by O. Bersillon, F. Gunsing, E. Bauge, R. Jacqmin, and S. Leray (EDP Sciences, Les Ulis, France, 2008), pp. 211–214. http://www.talys.eu
[12] R. Pachuau, B. Lalremruata, N. Otuka, L. R. Hlondo, L. R. M. Punte, and H. H. Thanga, Nucl. Sci. Eng. **187**, 70 (2017).
[13] http://www.epen.nhergmzu.com/epen/
[14] K. Abusaleem and B. Singh, Nucl. Data Sheets **112**, 133 (2011).
[15] H. Xiaolong, Nucl. Data Sheets **110**, 2533 (2009).
[16] J. Blachot, Nucl. Data Sheets **113**, 2391 (2012).
[17] N. Otuka, B. Lalremruata, M. U. Khandaker, A. R. Usman, and L. R. M. Punte, Radiat. Phys. Chem. **140**, 502 (2017).
[18] N. Otuka, B. Lalremruata, M. U. Khandaker, A. R. Usman, and L. R. M. Punte, Radiat. Phys. Chem. **149**, 151 (2018).
[19] A. D. Carlson, V. G. Pronyaev, D. L. Smith, N. M. Larson, Z. Chen, G. M. Hale, F.-J. Hambsch, E. V. Gai, S.-Y. Oh, S. A. Badikov, T. Kawano, H. M. Hofmann, H. Vonach, and S. Tagesen, Nucl. Data Sheets **110**, 3215 (2009).
[20] T. Sato, Y. Iwamoto, S. Hashimoto, T. Ogawa, T. Furuta, S. Abe, T. Kai, P. E. Tsai, N. Matsuda, H. Iwase, N. Shigyo, L. Sihver, and K. Niita, J. Nucl. Sci. Technol. **55**, 684 (2018).
[21] R. Capote, M. Herman, P. Obložinský, P. G. Young, S. Goriely, T. Belgya, A. V. Ignatyuk, A. J. Koning, S. Hilaire, V. A. Plujko, M. Avrigeanu, O. Bersillon, M. B. Chadwick, T. Fukahori, Zhigang Ge, Yinlu Han, S. Kailas, J. Kopecky, V. M. Maslov, G. Reffo, M. Sin, E. Sh. Soukhovitskii, and P. Talou, Nucl. Data Sheets **110**, 3107 (2009).
[22] A. J. Koning and J. P. Delaroche, Nucl. Phys. A **713**, 231 (2003).
[23] W. Hauser and H. Feshbach, Phys. Rev. **87**, 366 (1952).
[24] S. Hilaire, M. Girod, S. Goriely, and A. J. Koning, Phys. Rev. C **86**, 064317 (2012).
[25] J. Kopecky and M. Uhl, Phys. Rev. C **41**, 1941 (1990).
[26] D. M. Brink, Nucl. Phys. **4**, 215 (1957).
[27] P. Axel, Phys. Rev. **126**, 671 (1962).
[28] S. Goriely, Phys. Lett. B **436**, 10 (1998).

Correction: The first displayed equation in Sec. IV contained a minor error and has been fixed.